

## Technical Notes

# Analysis and Modelling on Radiated Noise of a Typical Fishing Boat Measured in Shallow Water Inspired by AQUO Project's Model

Zilong PENG, Jun FAN, Bin WANG

*Shanghai Jiao Tong University*

*Collaborative Innovation Center for Advanced Ship and Deep-Sea Exploration*

*State Key Laboratory of Ocean Engineering*

Shanghai 200240; e-mail: zlp\_just@sina.com; fanjun@sjtu.edu.cn; ellips.wang@hotmail.com

(received May 8, 2017; accepted January 10, 2018)

The shipping noise near channels and ports is an important contribution to the ambient noise level, and the depth of these sites is often less than 100 m. However less attention has been paid to the measurement in shallow water environments (BROOKER, HUMPHREY, 2016). This paper presents extensive measurements made on the URN (underwater radiated noise) of a small fishing boat in the South China Sea with 87 m depth. The URN data showed that the noise below 30 Hz was dominated by the background noise. The transmission loss (TL) was modelled with FEM (finite element method) and ray tracing according to the realistic environmental parameters *in situ*. The discrepancy between the modelled results and the results using simple law demonstrates both sea surface and bottom have significant effect on TL for the shallow water, especially at low frequencies. Inspired by the modelling methodology in AQUO (Achieve QUIeter Oceans) project (AUDOLY *et al.*, 2015), a predicted model applied to a typical fishing boat was built, which showed that the URN at frequencies below and above 100 Hz was dominated by non-cavitation propeller noise and mechanical noise, respectively. The agreement between predicted results and measured results also demonstrates that this modelling methodology is effective to some extent.

**Keywords:** radiated noise; South China Sea; predicted model; shallow water; transmission loss.

### 1. Introduction

During the past decades, ambient noise became an active area of research. Heightened concerns are evident from the increase of scientific and popular articles devoted to marine mammal stranding. The most sensitive and controversial yet least understood subject is the effect of human-generated noise on marine mammals (BOARD, 2003). The ambient noise from about 10 Hz to a few hundred Herz is dominated by the shipping noise (WENZ, 1962).

In addition to the above reasons, the ambient noise is a kind of background interference for the active or passive detection of underwater targets (AINSLIE, 2010). With the improved stealth capability of submarines, lowering the target strength (TS) at low frequencies faces a new challenge. One of the most urgent issues is further studying on the low-frequency ocean ambient noise characteristics.

So far, there are many models proposed to predict URN, which can be divided into two categories.

One is based on the statistical regularity from lots of measured samples, and the other is based on the shipping noise mechanism combining the contribution due to machinery, propeller, and cavitation. Of which, the two earliest predicted models are proposed by ROSS (1987) and URICK (1983), respectively. They derived the shipping noise level expressed as a function of frequency, ship length, draught, and speed. Later, WALES and HEITMEYER (2002) proposed the mean spectrum model describing the source spectra between 30 Hz and 1200 Hz of ships in the Mediterranean Sea and the eastern Atlantic Ocean. In the RANDI-2 model (HAMSON, 1994; 1997), an “average” ship’s source level can be obtained from the mean curve firstly, and the source level for each individual ship can be calculated as a function of its speed and length. On this basis, an updated version called the RANDI-3 model was developed (BREEDING *et al.*, 1996).

Different from the above models, WITTEKIND (2014) proposed a simple model for URN of the merchant ship. The URN can be decomposed into three

components: the low-frequency propeller noise, the high-frequency propeller noise, and the diesel engine noise. The input parameters include ship speed, cavitation inception speed, block coefficient, displacement, and the mass and number of engines.

By comparing the source levels of one ship (length 150 m, draught 4 ktons, speed 14 kt) predicted by different models, large deviations were found in the AQUO project (AUDOLY *et al.*, 2015). They concluded that “one possible interpretation is that some of these models (in particular Urick’s model) are established a long time ago, with a majority of vessels from the 2nd world war period”. On that basis, they proposed a URN model, in which the source level is decomposed into three components similar to the Wittekind’s model. The parameters were obtained by the numerical process of minimising the objective function, which needs at least two different speeds.

In this study, extensive measurements were made on the URN of a small fishing boat (length 43 m, displacement 500 tons) at South China Sea adhering to the American National Standards Institute/Acoustical Society of America S12.64-2009 standard (ANSI/ASA; 2009a; 2009b) as much as possible. This paper is organised as follows: In Sec. 2, we briefly introduced the target vessel and measurement conditions. Then we presented the data processing methodology, analysed the noise tonal components at low frequencies and the mechanism of spectrogram. Based on the principle of reciprocity, we presented a simulation case almost completely approaching reality based on 2D-axisymmetric FEM. In Sec. 3, we analysed the background noise. According to the realistic geoacoustic parameters *in situ*, we estimated the TL using FEM and ray tracing. Furthermore, we discussed and analysed the TL results in shallow water. On this basis, we presented the source level (SL) in Narrow band spectrum and 1/3 octaves spectrum. In Sec. 4, we firstly introduced the methodology of AUQO project model and made the corresponding adjustment. Then we presented the predicted model applied to a typical fishing boat. Finally, a summary and a discussion of the results were presented in Sec. 5.

## 2. Measurement and data processing methodology

### 2.1. Description of target vessel and measurement conditions

The measurements of radiated noise from the target vessel were undertaken by Shanghai Jiao Tong University (SJTU) and the Institute of Acoustics of the Chinese Academy of Sciences (IOA, CAS) in May, 2015. As the 87 m depth *in situ* was too low to meet the minimum water depth requirements in the ANSI S12.64-2009 standard, a bottom-mounted acoustic ob-

servatory containing an autonomous hydrophone was designed to estimate the SL of the target vessel. The acoustic observatory was implemented approximately 100 nautical miles off the coast of China.

The target vessel during the trials is pictured in Fig. 1. It is now applied to doing research reconstructed by a fishing boat. Table 1 provides a specification of the vessel. During the trials, the target vessel was operated along the straight line about 100 m away from the receiver, according to recommended published standards, as illustrated in Fig. 1. But in fact, as the effect of ocean current and also to avoid the propeller blades to encounter the rope of spar buoy, it was impossible to move along a straight line during the operation. The real closest distances of all runs will be introduced in Subsec. 3.2 (shown in Fig. 8).

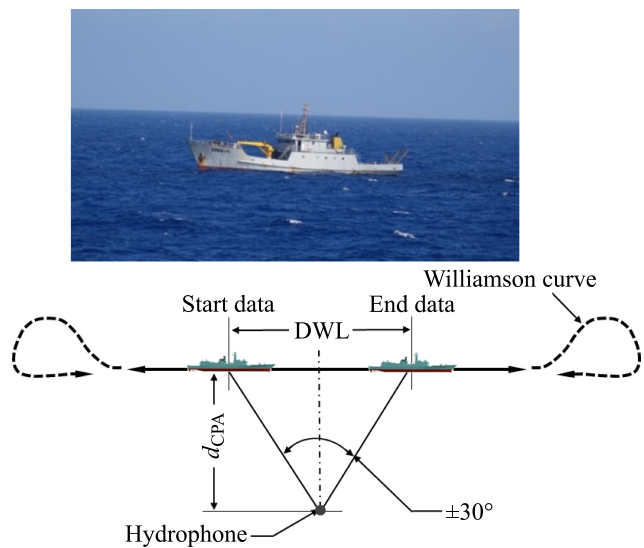


Fig. 1. Photography of the target vessel.

Table 1. Specification of the target vessel.

Length overall	43 m
Beam	8 m
Deadweight tons (DWT)	500 t
Draft	2.6 m (stem)/3.6 m (aft)
Speed range	5 ~ 9 kt
Number of blades	4
Propeller diameter	1.9 m
Engine mass	3800 kg
Engine power, maximum	430 kW
Engine type	750 rpm, 8 cylinders, 4-stroke
Ship’s service generator	Diesel, 4 cylinders, 4-stroke

The layout of acoustic observatory is shown in Fig. 2. The bottom-mounted receiver was fastened with a rope whose other end was tied to a spar buoy equipped with an Automatic Identification System

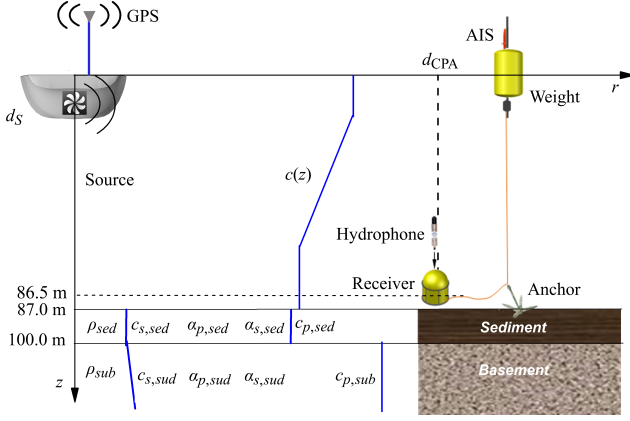


Fig. 2. Sketch of the acoustic observatory layout and geo-acoustic model *in situ*.

(AIS) system. The distance of the hydrophone from the bottom was about 0.5 m. In addition, another Global Positioning System (GPS) was set up to the target vessel to record its tracks accurately. The GPS data were subsequently used to determine the closest point of approach (CPA) distance and the data analysing window during its post-processing. The interior of the bottom-mounted hydrophone was equipped with a processor and memory, and the exterior was charged with batteries to fulfill the long-time data collection task underwater. The sensitivity of the hydrophone was  $-151$  dBV re  $\mu\text{Pa}$ , and its sampling rate was set as 48 kHz. Each data file recorded 30-min radiated noise data.

Furthermore, the experimental area can be characterised as a flat, roughly 87 m deep bottom. The sea floor is composed of a 13 m thick layer of clay and a half infinite layer of sand (LI, 2012; SHEPARD *et al.*, 1949), as shown schematically in Fig. 2. The TL modelling and other environmental parameters will be introduced and discussed in Subsec. 3.2.

### 2.2. Data processing methodology and spectrogram analysis

The spatial positions of the target vessel change constantly during the trials. This causes errors while attempting to determine its position at each moment due to lack of steady alignments between the CPA time given by AIS and the hydrophone clocks. However, the CPA must be present at the centre of the bathtub pattern in the spectrogram. Therefore, according to the passing characteristics of the time domain pattern or spectrogram shown in Fig. 3 and Fig. 4, we can define the data window period.

In order to obtain the power spectral density and 1/3 octaves spectrum, the recorded signal is processed as recommended in (SIMARD *et al.*, 2013). It should be noted that the spectrum is evaluated following the Welch procedure, a modified periodogram method widely used.

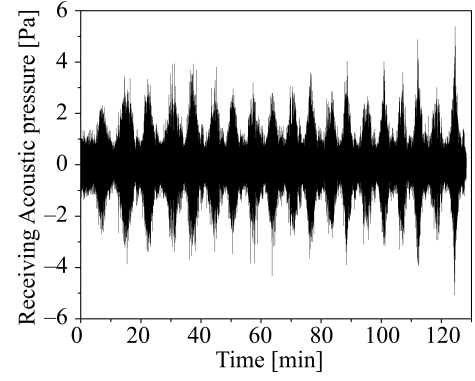


Fig. 3. Passing characteristic pattern of each run.

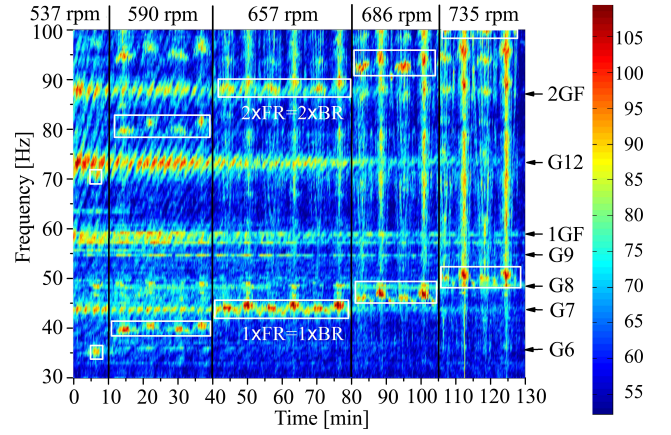


Fig. 4. Spectrogram of the vessel radiated noise for each pass with bandwidth 1 Hz.

As illustrated in Fig. 3, the passing characteristic pattern of each run (the speed of the target vessel is  $\sim 5-9$  kt) is clearly presented in the collected data (about 130 min). After filtering and performing the spectral analysis, the spectrogram of the radiated noise at frequencies below 100 Hz is obtained as shown in Fig. 4.

From Fig. 4, a series of bathtub striations are present, which are mainly caused by the interferences between the direct wave and reflection wave from the sea surface or sea bottom. Furthermore, the trajectory of a moving target is given by

$$R_o^2 = \left( \frac{2hd}{nc} \right)^2 f_n^2 - v^2 t^2, \quad n = 1, 2, L, \quad (1)$$

where  $R_o$  is the range at CPA,  $h$  and  $d$  are the depths of receiver and source [m], respectively;  $v$  and  $t$  are the speed [m/s] and time [s], respectively.  $f_n$  and  $c$  are the nulled frequency [Hz] and sound speed [m/s], respectively. Besides,  $t = 0$  is taken as the time of CPA. Thus, these striations have the shape of hyperbolae (KAPOLKA *et al.*, 2008).

Here we give a simulation case almost approaching reality based on 2D-axisymmetric FEM, supposing the speed of a moving target is 2.5 m/s (about 5 kt),

and the sound speed is taken from Fig. 9 (Subsec. 3.2). The geoacoustic parameters are given in Fig. 2 (Subsec. 2.1) and Table 2 (Subsec. 3.2). The moving target source intensity is considered as an omnidirectional point source with certain intensity, SL at 5 kt in Fig. 15 (Subsec. 3.3), situated 2.4 m below the surface. The depth of the receiver is 86.5 m. According to the principle of reciprocity, as indicated in Fig. 5, the calculated amount can be greatly reduced.

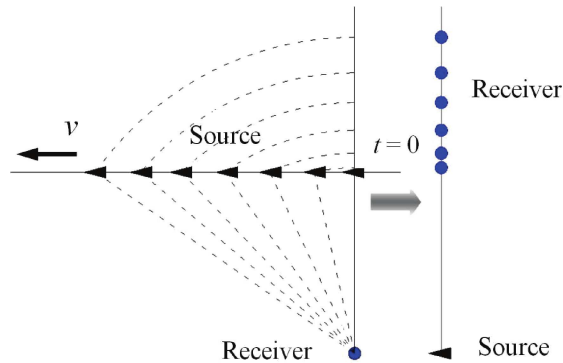


Fig. 5. Spectrogram modelling sketch of a moving target based on the principle of reciprocity.

As illustrated in Fig. 6, the modelling based on FEM can give the interference striations apparently. This method can also be available to higher frequency using ray tracing. Besides, the levels around 50 Hz are prominent due to the peak value in SL at 5 kt. However, the modelling result is not accurate enough inevitably, as it ignores the directionality of the source and tonal component.

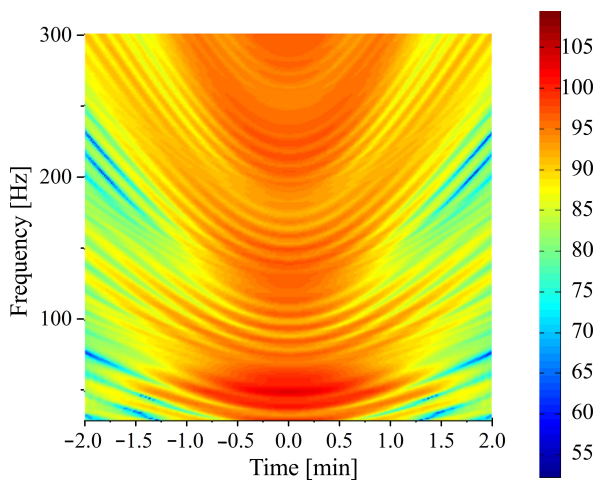


Fig. 6. Frequency vs. time spectrogram modelling result with 5 kt speed.

Furthermore, from Fig. 4, the radiated noise below 100 Hz can be characterised by tonal components and wide band noise. The strong tonal components appear below 100 Hz clearly, and are generally associated with the activity of the ship's mechanisms (e.g., main engine, service diesel generator, and propeller) and com-

plex varying characteristics of the speed (KOZACZKA, GRELOWSKA, 2004; GRELOWSKA *et al.*, 2013). The frequency lines generated by the main engine and propeller blade vary regularly due to the ship speed or rotating speed. As the vessel is powered by a four-stroke 8-cylinder diesel engine and with propulsion of a four-blade propeller, the diesel firing rate and blade rate can be defined as

$$FR = \frac{8 \times \text{rpm}}{60 \times 2} = \frac{4 \times \text{rpm}}{60} = BR. \quad (2)$$

Different from the frequency lines generated by the main engine and propeller blade, the frequency lines (a series of 6-Hz harmonics) generated by the service diesel generator (SDG) are independent of the ship speed. Five of these harmonics, at 36, 42, 48, 54, and 72 Hz, are strong enough to be contributors to the signature, as can be seen in Fig. 4.

The spectral source level (referenced to 1 m) of the target vessel is estimated from the received level (RL) at a distant range ( $R$ ), which is compensated for the TL according to the following equation,

$$SL(f) = RL(f, R) + TL(f, R), \quad (3)$$

where  $f$  and  $R$  are frequency [Hz] and the slant range along the propagation path [m], respectively.

There are two ways to compute the TL: modelling activities and simple law (AUDOLY *et al.*, 2015). The modelling activities require the input of environmental parameters, including bathymetry of the test site, source depth, and sound speed profile. The commonly used modelling methods include normal modes, ray tracing, parabolic equation, wave-number integration, and FEM (JENSEN *et al.*, 2011). Besides, simple laws such as spherical spreading, cylindrical spreading, and others are sometimes very useful, although they are rough handlings. Different from the above methods, WESTON (1971) presented a series of TL simple formulae to interpret the effect of range, frequency, water depth and bottom for constant-depth isovelocity water. Here, the TL will be modelled based on realistic geoacoustic parameters using FEM and ray tracing considering the calculation accuracy. The TL calculation will be discussed in Subsec. 3.2.

### 3. Results and analysis

#### 3.1. Background noise

During the measurement of the URN of the target vessel, the signal-to-noise ratio (SNR) depends on the background noise, which is always present. As recommended in ISO and ANSI standards, if the difference between the radiated noise and the background noise level is greater than 10 dB, the effect of background will be ignored. If the difference is less than 3 dB, the data is considered unusable. If the difference is between

3 dB and 10 dB, the correction will be made on the measured data as follows:

$$\text{Correction [dB]} = 10 \lg \left( \frac{10^{0.1\text{SNR}}}{10^{0.1\text{SNR}} - 1} \right). \quad (4)$$

In principle, measurement of the background noise should be made at the beginning and at the end of the each run, as the background noise isn't sufficiently stationary. Figure 7 shows an example of received Power Spectral Density (PSD) levels with 1 Hz bandwidth for various speeds and measured background noise. The background noise is measured at the end of the last run and about 10 min after the target vessel ran far away from the receiver. As indicated in Fig. 5, the spectrums of different speeds at low frequencies below approximately 30 Hz are nearly dominated by the background noise, and this phenomenon is also found and interpreted in (BROOKER, HUMPHREY, 2016). With the speed increases, the radiated noise of the target vessel will be enhanced and the effect of background noise will become weaker. So the data below 30 Hz are considered unusable and will not be discussed in modelling in the following sections.

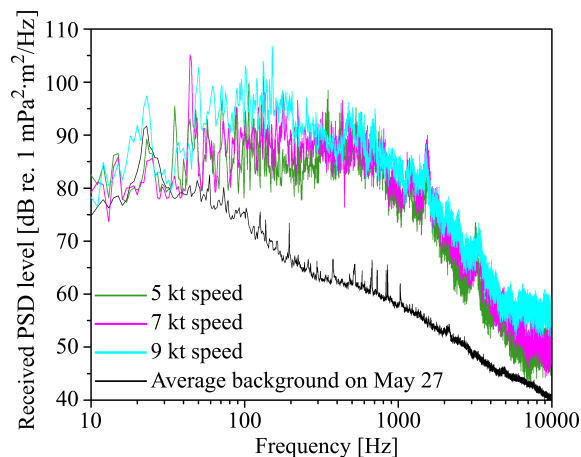


Fig. 7. Received PSD levels for various vessel speeds and measured background noise with 1 Hz bandwidth.

### 3.2. Transmission loss modelling

In spite of the CPA distance of 100 m recommended by ANSI standards, operating the target vessel along straight line was almost impossible due to the effect of the ocean current and the need to avoid the propeller blades encountering the rope of spar buoy. Figure 8 shows the real closest distances of all runs. When the vessel passes the receiver on the larboard, the CPA distances are about 180 m. Otherwise, the CPA distances are about 280 m.

As mentioned above, the TL computation requires some environmental parameters. Figure 9 shows the sound speed profile *in situ*. The speed profile belongs to the typical 3-layer mid-latitude summer profile in shallow water, i.e., a surface mixed layer,

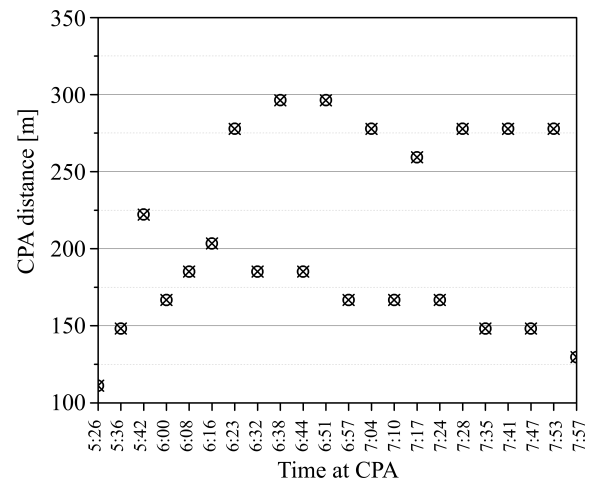


Fig. 8. Closest distances of all runs.

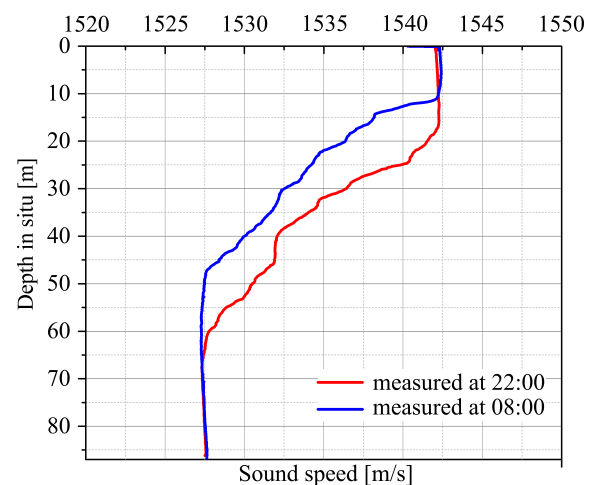


Fig. 9. Sound speed profile *in situ*.

a thermocline, and a bottom mixed layer. The sound speed near the bottom is about 15 m/s lower than that near the surface. Furthermore, the temperature decreases in the night make the sound speed at the same depth in the morning lower than that in the night. Thus, the thermocline and surface mixed layer become shallow, and the range of bottom mixed layer is enlarged.

The depth of source is generally considered as two thirds of draft (AUDOLY *et al.*, 2015). Hence, the point source is set as 1 Pa at 1m with 2.4 m depth below the surface. The geoacoustic model and experimental configuration have been introduced in Subsec. 2.1 and shown in Fig. 2. The corresponding geoacoustic parameters (JENSEN, 2000; HAMILTON, 1980) are listed in Table 2.

For frequencies lower than 1 kHz, the acoustic pressure field is modelled with 2D-axisymmetric FEM. To model the sound propagation in semi-infinite medium, Perfect Matched Layer (PML) is used in FEM modelling with COMSOL. For frequencies from 1 kHz to 10 kHz, the acoustic pressure field can be modelled

Table 2. Geoacoustic parameters description.

Description	Symbol	Value
Sediment: clayey silt		
Comp. speed [m/s]	$c_{p, sed}$	1500
Comp. attenuation [dB/ $\lambda_p$ ]	$\alpha_{p, sed}$	0.2
Shear wave speed [m/s]	$c_{s, sed}$	80
Shear attenuation [dB/ $\lambda_s$ ]	$\alpha_{s, sed}$	1.0
Density [g/cm <sup>3</sup> ]	$\rho_{sed}$	1.5
Subbottom: fine sand		
Comp. speed [m/s]	$c_{p, sub}$	1650
Comp. attenuation [dB/ $\lambda_p$ ]	$\alpha_{p, sub}$	0.8
Shear wave speed [m/s]	$c_{s, sub}$	110z <sup>0.3</sup>
Shear attenuation [dB/ $\lambda_s$ ]	$\alpha_{s, sub}$	2.5
Density [g/cm <sup>3</sup> ]	$\rho_{sub}$	1.9

using BELLHOP based on ray tracing. It should be noted that coherent TL calculation is chosen as the run type. The sediment and subbottom are regarded as fluid mediums, thus the shear waves and shear attenuation will be ignored in BELLHOP.

Figure 10 shows the TL patterns at 100 Hz, 1 kHz and 10 kHz [dB]. With the increase of frequency, the patterns show that the TL near the bottom varies more dramatically along the horizontal distance. Furthermore, we give the calculated TLs at different receiving horizontal distances. As illustrated in Fig. 11, the TLs at the same frequencies tend to increase with the horizontal distance.

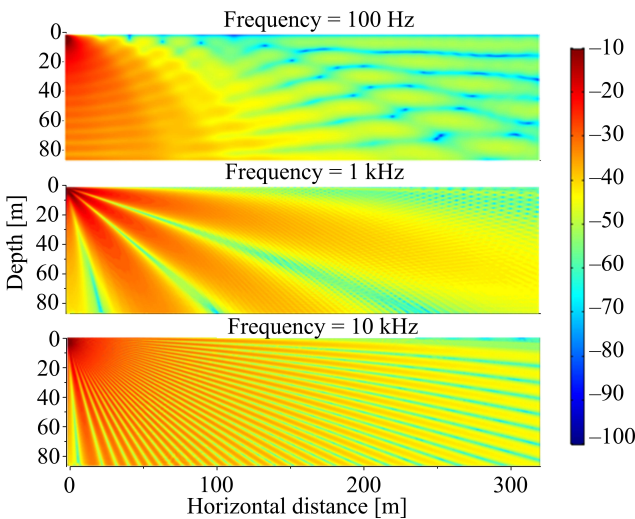


Fig. 10. TL patterns at 100 Hz, 1 kHz and 10 kHz.

Among these results, we choose the TL computations at 111.1 m and 296.3 m to study further, as shown in Fig. 12 and Fig. 13, respectively. Both narrow band spectrum results show that the TL estimated with mirror effect, only considering the sea surface, is close to the estimations with FEM and ray tracing based on the realistic environmental parameters at

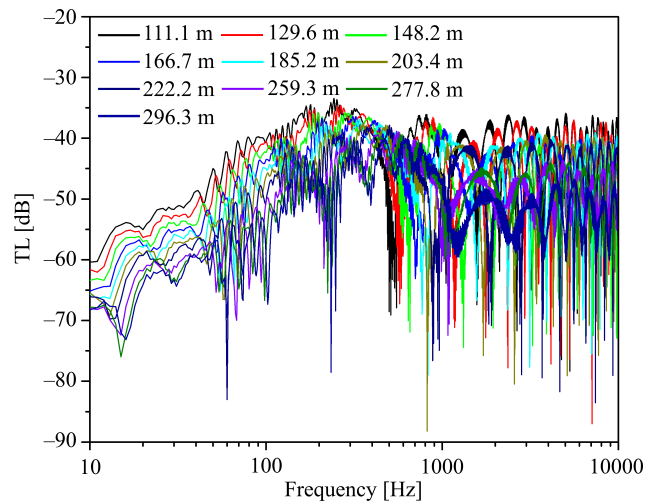


Fig. 11. TL computations at different receiving horizontal distances indicated in Fig. 6.

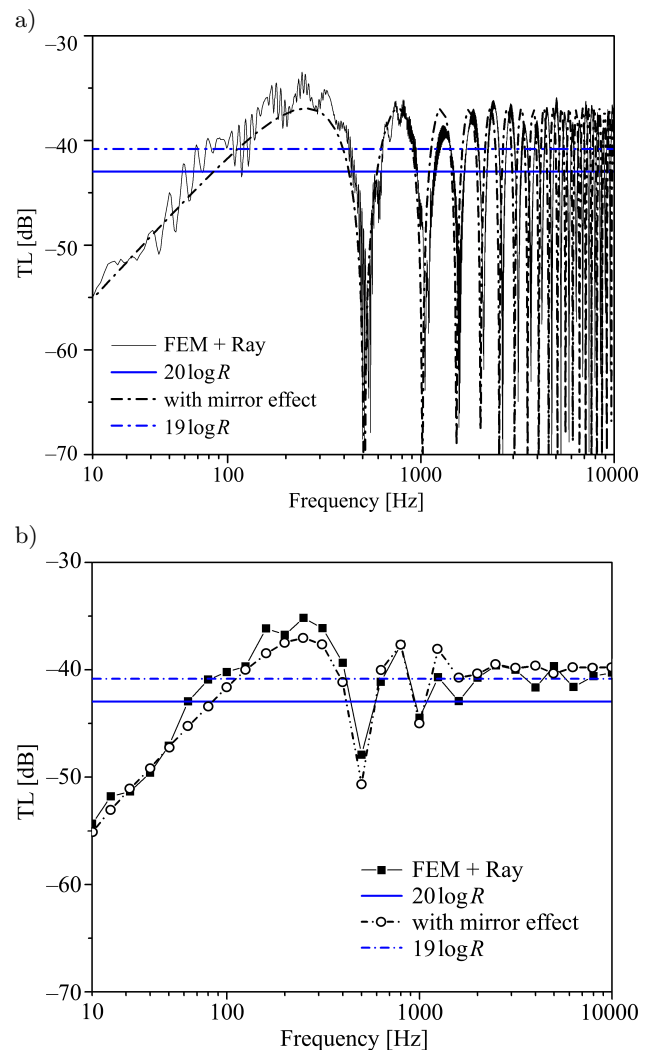


Fig. 12. TL computations with the receiving horizontal distance of 111.1 m: a) narrow band result with 1 Hz bandwidth; b) 1/3 octave band-averaged result.

frequencies below 1 kHz, and this effect is more pronounced for the closer distance to the source. The dis-

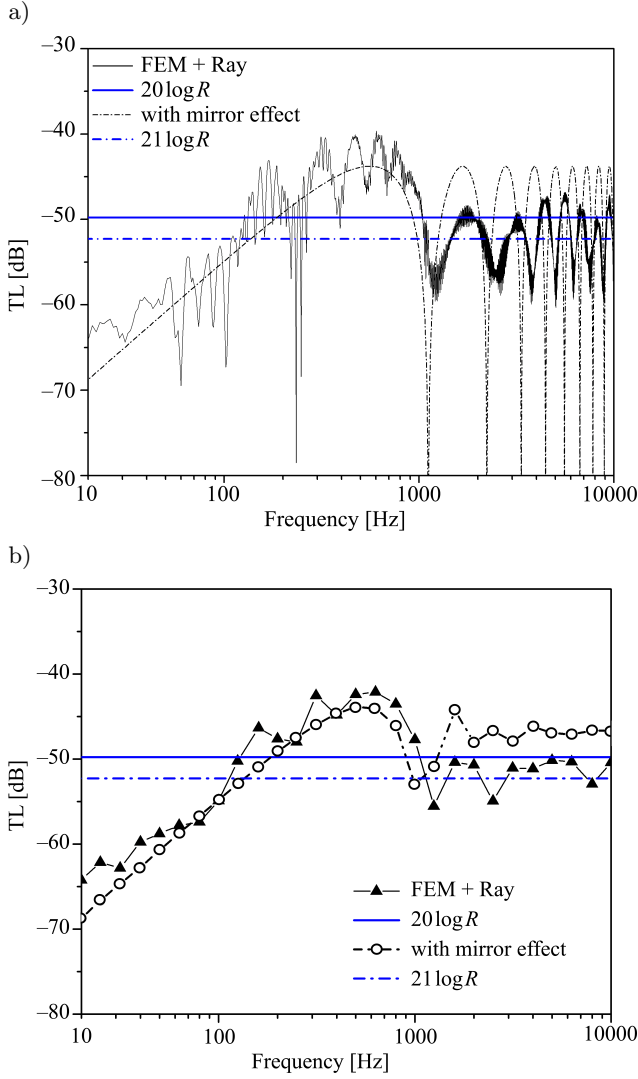


Fig. 13. TL computations with the receiving horizontal distance of 296.3 m: a) narrow band result with 1 Hz bandwidth, b) 1/3 octave band-averaged result.

crepancies between them will become dramatical for the higher frequencies. Besides, the valleys for the farther distance tend to be much smoother rather than sharp.

From the 1/3 octave band-averaged spectrums, the estimations with mirror effect are also very close to the calculated results with FEM and ray tracing within the whole frequency domain for the distance of 111.1 m, which indicates that the sea surface is the primary factor for the closer distances. The main reason may be that the negative sound speed gradient makes the sound bend towards the bottom with a certain attenuation effect. However, with increase of the receiving distance, the discrepancy becomes more dramatical as the sound encounters the reflections from the sea surface and bottom repeatedly. Thus, the realistic TLs are higher than that with the mirror effect. Besides, the TL estimation in 1/3 octaves with

FEM and ray tracing tends to be at a stable level. To be more specific, for the frequencies above 1 kHz, the TLs at 111.1 m and 296.3 m are close to  $19\lg R$  and  $21\lg R$ , respectively. In the same way, we conclude that the TLs at frequencies above 1 kHz with the horizontal distance from 111.1 m to 296.3 m are from  $19\lg R$  to  $21\lg R$ . That is to say, for the high frequencies and closer ranges, TL can be estimated with a simple law.

### 3.3. SL in narrow band spectrum and 1/3 octaves spectrum

There are two general methods to depict the source level measurement: monopole method and equivalent source method (Ainslie, 2010). As our measurement is carried out in shallow water, which can bring in multiple reflections from the surface and bottom, it is difficult to depict using the equivalent source method. On the contrary, the monopole source method can give consistent results for various environments (COWARD, 2013), therefore, we use the latter in this study. Recall that TL computations have been given in Subsec. 3.2. On the one hand, if we use the narrow band result, a series of valleys will result in some false peaks present in the SL in the narrow band spectrum. On the other hand, as interpreted and recommended in AQUO project report (AUDOLY *et al.*, 2015) and AINSLIE's work (2010), the relationship between the monopole method and equivalent source method is given by:

$$SL_{\text{corr}}(f, V, L) = SL(f, V, L) + \text{Max} \left[ 0; 10 \lg \left( \frac{1}{2} + \frac{1}{(2(2\pi f/c) z_s(L) \sin \theta)^2} \right) \right], \quad (5)$$

where  $SL_{\text{corr}}$  and  $SL$ , in fact, are SL in the monopole method and equivalent method, respectively;  $V$  and  $L$  are the speed [kt] and ship length [m];  $\theta$  is the depression or "look down" angle relative to the surface;  $z_s$  is the depth of source.

The SL in the equivalent method can be replaced by the following form:

$$SL(f, V, L) = RL(f, V) + n(f, L) \lg R, \quad (6)$$

where  $n$  is the coefficient of TL using the simple law.

Substituting Eq. (6) into Eq. (5) and combining with Eq. (3), we obtain the transmission loss in the monopole method as follows:

$$TL_{\text{corr}}(f, V, L) = n(f, L) \lg R + \text{Max} \left[ 0; 10 \lg \left( \frac{1}{2} + \frac{1}{(2(2\pi f/c) z_s(L) \sin \theta)^2} \right) \right], \quad (7)$$

where the second term on the right represents the excess of TL considering the Lloyd's mirror effect than that using the simple law. But for shallow water, this

low-frequency correction should include the bottom effect. Hence, we use 1/3 octave band-averaged PL at the low frequencies. For the higher frequencies, as illustrated in Figs. 12b and 13 b, it is reasonable to use a simple law,  $19\sim 21\lg R$ , to model the TL.

The measurements of radiated noise at different speeds are always repeated several times to ensure that the results are consistent. The radiated noise level is obtained by averaging the data of repeated times. Thus, on the basis of TL computations, we obtain the SL in the narrow band spectrum and 1/3 octaves spectrum, as shown in Figs. 14 and 15. It should be emphasised that the SLs in the narrow band spectrum are chosen from the measured data according to different speeds [kt]. Because the realistic speeds cannot be guaranteed to be completely the same even for the same speed [kt], the tonal components will be meaningless after averaging.

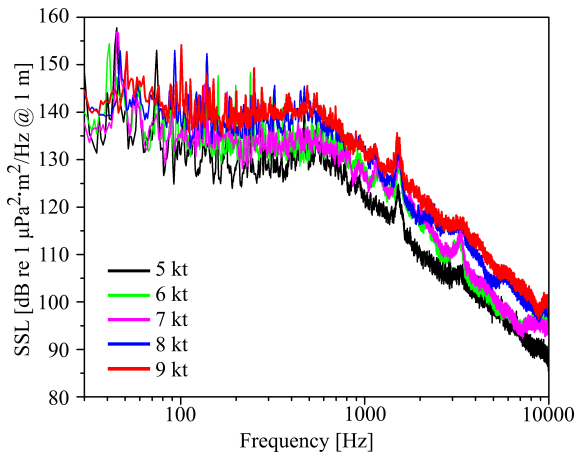


Fig. 14. SLs in the narrow band spectrum with bandwidth 1 Hz chosen from the measured data.

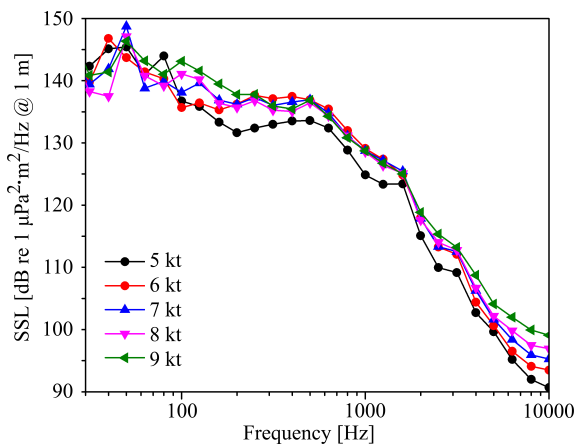


Fig. 15. SL in 1/3 octaves spectrum after averaging the data of repeated times.

As indicated in Figs. 14 and 15, the high-level noise below 100 Hz is mainly contributed by the mechanical

noise (e.g. main engine and service diesel generator) and propeller noise, and complex varying characteristics of the speed, which has been discussed in Subsec. 2.2. With the increase of speed, the SLs are enhanced obviously.

## 4. URN predicted model

### 4.1. Methodology of AQUO project's model

In the AQUO project's model (AUDOLY *et al.*, 2015), the radiated noise can be decomposed into three components: low-frequency propeller noise, high-frequency propeller noise, and mechanical noise. Thus, the spectral source level of target vessel can be expressed as:

$$SL_{TOT}(f, V) = 10 \lg \left( 10^{0.1SL_{mach}(f, V)} + 10^{0.1SL_{prop}(f, V)} + 10^{0.1SL_{cav}(f, V)} \right), \quad (8)$$

where  $SL_{TOT}$  is the total SL [dB];  $SL_{mach}$ ,  $SL_{prop}$ , and  $SL_{cav}$  are the SL [dB] related mechanical noise, low-frequency propeller noise, and high-frequency propeller cavitation noise, respectively.

Each term of the different noises can be described by characteristic patterns depending on frequency and speed affect to unknown coefficients for a given vessel (AUDOLY *et al.*, 2015):

$$\begin{aligned} SL_{mach} &= K_1 + K_4 \lg V, & f < f_{mach}, \\ SL_{mach} &= K_2 + K_3 \lg f + K_4 \lg V, & f > f_{mach}, \\ SL_{prop} &= K_5 + K_6 \lg f + K_9 \lg V, & f < f_{prop}, \\ SL_{prop} &= K_7 + K_8 \lg f + K_9 \lg V, & f > f_{prop}, \\ SL_{cav} &= K_{10} + K_{11} \lg f + K_{12} \lg V, & f < f_{cav}, \\ SL_{cav} &= K_{13} + K_{14} \lg f + K_{12} \lg V, & f > f_{cav}. \end{aligned} \quad (9)$$

In order to determine the 17 unknown coefficients ( $K_1, \dots, K_{14}, f_{mach}, f_{prop}$ , and  $f_{cav}$ ), the continuity conditions are imposed at the characteristic frequencies  $f_{mach}$ ,  $f_{prop}$  and  $f_{cav}$

$$\mathbf{A}_{equ} \mathbf{K} = \mathbf{0}, \quad (10)$$

where  $\mathbf{A}_{equ}$  is a  $3 \times 14$  matrix in which  $a_{11}, a_{25}, a_{3,10} = 1, a_{12}, a_{27}, a_{3,13} = -1, a_{13} = -\lg f_{mach}, a_{26} = \lg f_{prop}, a_{28} = -\lg f_{prop}, a_{3,11} = \lg f_{cav}, a_{3,14} = -\lg f_{cav}$ , and other elements are 0;  $\mathbf{K} = (K_1, \dots, K_{14})^T$ ;  $\mathbf{0} = (0, 0, 0)^T$ .

In addition, some restrictive conditions about typical values are also imposed on some parameters to improve the numerical efficiency and avoid unreasonable results, which is suggested by ROSS (1987) and can be found in (AUDOLY *et al.*, 2015). For example, the

factor  $K_3$  with respect to the logarithm of frequency has a typical value of  $-7$  to  $-8$  dB per octave (or typically  $-25$  dB per decade). The dependence of levels with speed,  $K_4$ , is not expected to increase more than 30 times the logarithm. Considering a deviation with  $\pm 5$  dB, these restrictive conditions about typical values are listed as follows:

$$\begin{aligned} -30 < K_3 < -20, & & 20 < K_4 < 30, \\ -35 < K_8 < -25, & & 45 < K_9 < 55, \\ 0 > K_6 > K_8, & & 15 < K_{11} < 25, \\ 55 < K_{12} < 65, & & -25 < K_{14} < -15. \end{aligned} \quad (11)$$

The above equations can be rewritten in a matrix form:

$$\mathbf{A}\mathbf{K} < \mathbf{b}, \quad (12)$$

where  $\mathbf{A}$  is a  $16 \times 14$  matrix in which  $a_{13}, a_{34}, a_{58}, a_{79}, a_{10,6}, a_{11,11}, a_{13,12}, a_{15,14} = -1$ ,  $a_{23}, a_{44}, a_{68}, a_{89}, a_{96}, a_{10,8}, a_{12,11}, a_{14,12}, a_{16,14} = 1$ , and other elements are 0;  $\mathbf{b} = (30, -20, -15, 35, -25, -45, 55, 0, -15, 25, -55, 65, 25, -15)^T$ ;  $\mathbf{b} = (30, -20, -20, 30, 35, -25, -45, 55, 0, 0, -15, 25, -55, 65, 25, -15)^T$ .

Finally, the numerical process can be written as this task: finding the 17 unknown coefficients ( $K_1, \dots, K_{14}, f_{\text{mach}}, f_{\text{prop}}$ , and  $f_{\text{cav}}$ ) such as the below objective function is minimised,

$$\sum_{m=1}^M \sum_{q=1}^Q \left| \text{SL}_{\text{exp}}(f_q, V_m) - 10 \lg \left( 10^{0.1 \text{SL}_{\text{mach}}(f_q, V_m)} + 10^{0.1 \text{SL}_{\text{prop}}(f_q, V_m)} + 10^{0.1 \text{SL}_{\text{cav}}(f_q, V_m)} \right) \right|, \quad (13)$$

where  $m$  and  $q$  are the sequences of speed and centre frequency of 1/3 octave band spectrum,  $\text{SL}_{\text{exp}}$  is the experimental value of SL.

#### 4.2. Noise modelling of the target vessel with the AQUO project's methodology

In order to improve the numerical efficiency, the three characteristic frequencies are ruled as the 1/3 octave frequencies from 50 Hz to 630 Hz successively. But as recommended by (AUDOLY *et al.*, 2015), the frequency  $f_{\text{cav}}$  corresponding to the maximum is generally between 50 Hz and 200 Hz. So the frequency  $f_{\text{cav}}$  is restricted to this frequency range. By doing triple “for loop”, the 17 unknown coefficients can be determined, so that the objective function is minimised. Here we choose the optimal solver, “fmincon” (constrained nonlinear minimisation) with “SQP” algorithm, to fulfill this task. According to Eq. (13), we obtained the formula of the radiated noise as follows,

$$\begin{aligned} \text{SL}_{\text{mach}}(f, V) &= 118.9 + 20 \lg V, & f < 500 \text{ Hz}, \\ \text{SL}_{\text{mach}}(f, V) &= 200.0 - 30 \lg f + 20 \lg V, & f > 500 \text{ Hz}, \\ \text{SL}_{\text{prop}}(f, V) &= 103.8 - 0.23 \lg f + 45 \lg V, & f < 80 \text{ Hz}, \\ \text{SL}_{\text{prop}}(f, V) &= 170 - 35 \lg f + 45 \lg V, & f > 80 \text{ Hz}, \\ \text{SL}_{\text{cav}}(f, V) &= -32.5 + 17.2 \lg f + 58 \lg V, & f < 125 \text{ Hz}, \\ \text{SL}_{\text{cav}}(f, V) &= 55.4 - 24.7 \lg f + 58 \lg V, & f > 125 \text{ Hz}. \end{aligned} \quad (14)$$

As illustrated in Fig. 16a, the predicted results are in close agreement with the experimental results. As the relationship between speed and SL of each component is assumed to be a simple and linear function, the predicted model cannot be accurate enough. From Fig. 12b, it is easy to find that the high-frequency propeller cavitation noise is much lower than other components, which provides an evidence that no cavitation occurs for the target vessel. Besides, another evidence is that no more than 10 dB increases in SL for every 1 kt increase in speed (Fig 15).

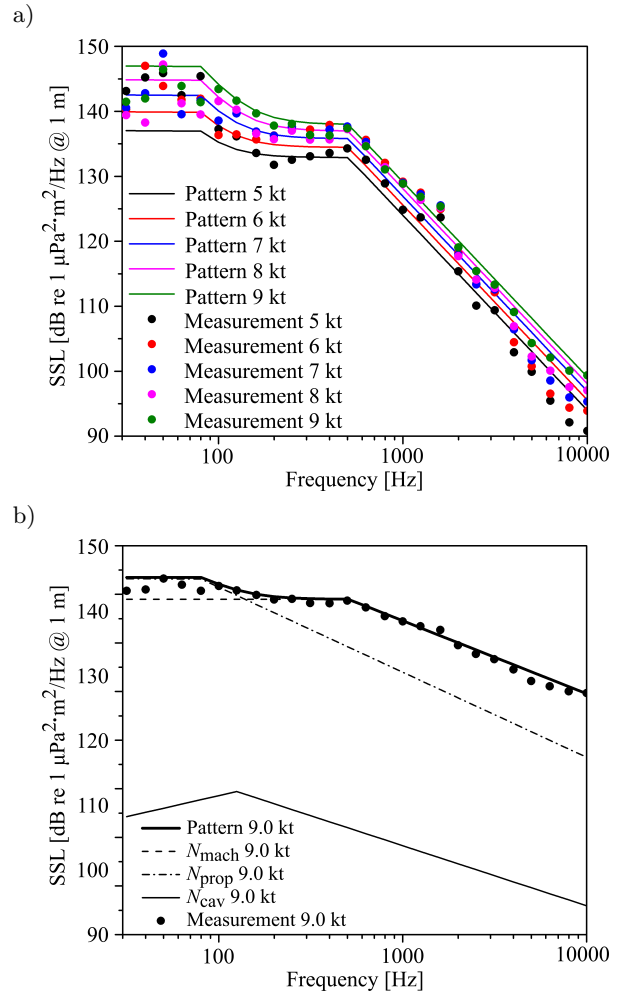


Fig. 16. Comparison between experimental results and predicted results: a) URN pattern optimisation for the target vessel; b) decomposition into noise components at 9 kt.

Therefore, the optimisation should be adjusted only considering the mechanical noise and non-cavitation propeller noise. The adjusted results are shown in Fig. 17. Almost nothing has changed in Fig. 17a as compared with Fig. 16a. Figure 17b indicates that the main component of the radiated noise is mechanical noise, which controls the frequency domain above 100 Hz, and the non-cavitation propeller noise plays an important role at low frequencies below 100 Hz. For the higher frequency above several hundred Hz, the propeller noise is difficult to distinguish from the mechanical noise. Furthermore, the predicted results with Ross's model at 5 kn and 9 kn are also presented in Fig. 17a. Here we give the Ross's model defined by the following equation,

$$SL(f, V) = 190 + 53 \lg(V/10) - 20 \lg f, \quad f > 100 \text{ Hz.} \quad (15)$$

From Fig. 17a, except for the frequencies around 500 Hz and 10 kHz, the measured source levels are within the predicted levels using Ross's model. Besides,

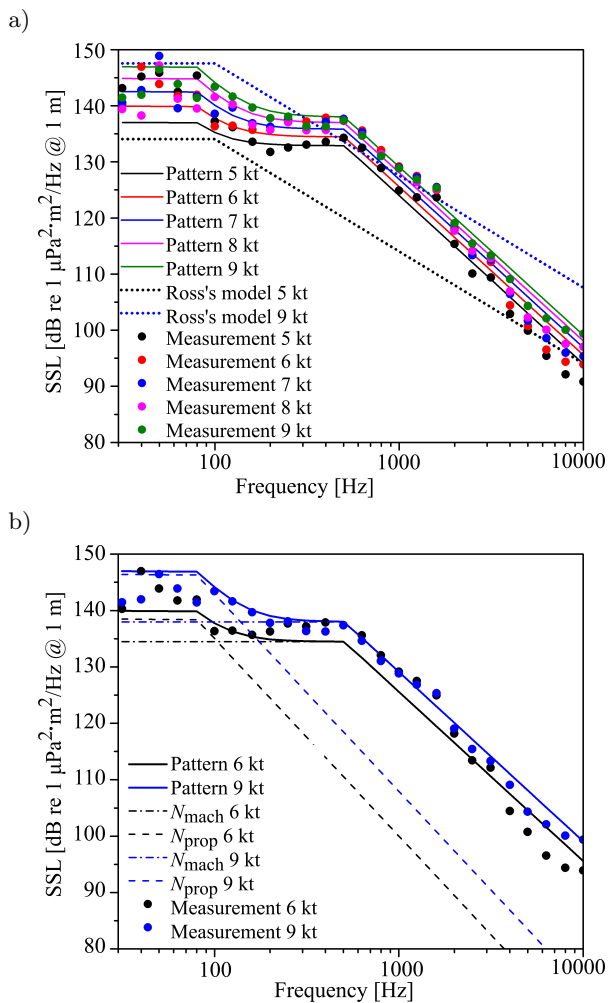


Fig. 17. Adjusted comparison results: a) URN pattern optimisation for the target vessel, b) decomposition into noise components at 6 kt and 9 kt, respectively.

the source levels of this vessel have a steeper slope ( $-30$  dB/decade) of frequency than that of Ross's model ( $-20$  dB/decade) above about 500 Hz. As indicated in Eq. (14), this slope mainly depends on the mechanical noise.

Judging from the above analysis, apparently, the components can be separated easily, which is the advantage of this methodology. But the noise component separation is a very complicated and tough problem. Sometimes, the optimal solving is not stable enough and sensitive to the samples and boundary definition. Therefore, it should be emphasised that this noise modelling based on AQUO project methodology has its limitation and needs further research.

## 5. Discussion and conclusions

The measurement of radiated noise from a target vessel complying with the ANSI standards is a challenging undertaking (BROOKER, HUMPHREY, 2016). Especially when the depth of an experimental site is less than 100 m, the measurement cannot meet the standards. On the other hand, the shipping noise near channels and ports is an important contribution to the ocean ambient noise level. Based on the above consideration, our acoustic observatory was equipped with an autonomous bottom-mounted hydrophone complying with standards as much as possible.

By making extensive measurements on the URN of the target vessel, we obtained the noise data at speeds from 5 kt to 9 kt. To ensure the validity of the noise data, background noise was measured and compared with shipping noise. The analysis of the results showed that the spectrums of different speeds at low frequencies below approximately 30 Hz were nearly dominated by the background noise.

For the measurement in shallow water, the transmission loss is very important and crucial. To obtain reliable TL, we adopted the modelling activity with FEM and ray tracing according to the realistic environmental parameters *in situ*. The modelling results show that there is a great discrepancy as compared to the simple law at low frequencies mainly due to the Lloyd's mirror effect. On this basis, the power spectral density and  $1/3$  octaves spectrum were computed after the recorded signal is processed.

Inspired by the methodology in AQUO project, we modelled the URN of target vessel using an optimal solver of constrained nonlinear minimisation. It has been found that the predicted results were in close agreement with the experimental results. The main component of the radiated noise was mechanical noise, which almost controlled the frequency domain above 100 Hz. But for the frequencies below 100 Hz, the non-cavitation propeller noise has a higher level. In addition, the modelling methodology inevitably needs to be ameliorated in the further research, as the relationships

between speed and frequency and each noise component are assumed to be a simple and linear function.

### Acknowledgments

This work was supported by Collaborative Innovation Center for Advanced Ship and Deep-Sea Exploration, SJTU and IOA. The data were obtained under the guidance of Prof. Xinyi Guo and Prof. Jinrong Wu of IOA. The photo of the fishing vessel is provided by Guoli Song of IOA. We appreciate their help. The first author would also like to thank his wife Chang Wu, Prof. Weilin Tang, Dr. Yunzhe Tong, Dr. Fulin Zhou, Dr. Kaiqi Zhao, and Dr. Bo Liu for their suggestions. Finally, we would like to thank the anonymous reviewers for the insightful comments and helpful suggestions made.

### References

- AINSLIE M.A. (2010), *Principles of sonar performance modelling*, Springer.
- ANSI/ASA (2009a), ANSI S1.11, *Specification for octave-band and fractional-octaveband analog and digital filters*.
- ANSI/ASA (2009b), S12.64-2009/Part 1 (R2014), *Quantities and Procedures for Description and Measurement of Underwater Sound from Ships – Part 1: General Requirements*.
- AUDOLY C., RIZZUTO E. (2015), *Ship underwater radiated noise patterns*, AQUO European Collaborative Project, Deliverable D2.1.
- AUDOLY C., ROUSSET C., RIZZUTO E., MULLOR R.S., HALLANDER J., BAUDIN E. (2015), *Mitigation measures for controlling the ship underwater radiated noise, in the scope of AQUO Project*, [in:] OCEANS 2015-Genova, pp. 1–6.
- BOARD O.S., (2003), *National Research Council. Ocean noise and marine mammals*, National Academies Press.
- BREEDING J.E., PFLUG L.A., BRADLEY M., HEBERT M., WOOTEN M. (1994), *RANDI 3.1 User's Guide* (No. NRL/MR/7176-94-7552), Naval Research Lab Stennis Space Center MS.
- BREEDING JR, J.E., PFLUG L.A., BRADLEY M., WALROD M.H. (1996), *Research Ambient Noise Directionality (RANDI) 3.1 Physics Description* (No. NRL/FR/7176-95-9628), Naval Research Lab Stennis Space Center MS.
- BROOKER A., HUMPHREY V. (2016), *Measurement of radiated underwater noise from a small research vessel in shallow water*, *Ocean Engineering*, **120**, 182–189.
- COWARD S. (2013), *A method for remote sensing of acoustic ship noise*, Master's Thesis, Norwegian University of Science and Technology, <http://hdl.handle.net/11250/23709>.
- COWARD S., TOLLEFSEN D., DONG H. (2013), *Radiated ship noise level estimates from measurements in a fjord*, *The Journal of the Acoustical Society of America*, **134**, 5, 4150–4150.
- GRELOWSKA G., KOZACZKA E., KOZACZKA S., SZYM-CZAK W. (2013), *Underwater noise generated by a small ship in the shallow sea*, *Archives of Acoustics*, **38**, 3, 351–356.
- HAMILTON E.L. (1980), *Geoacoustic modeling of the sea floor*, *The Journal of the Acoustical Society of America*, **68**, 5, 1313–1340.
- HAMSON R.M. (1994), *Sonar array performance prediction using the RANDI-2 ambient noise model and other approaches*, BAeSEMA Report B 1277/TR-1.
- HAMSON R.M. (1997), *The modelling of ambient noise due to shipping and wind sources in complex environments*, *Applied Acoustics*, **51**, 3, 251–287.
- JENSEN F.B., KUPERMAN W.A., PORTER M.B., SCHMIDT H. (2011), *Computational ocean acoustics*, Springer Science & Business Media.
- KAPOLKA D., WILSON J.K., RICE J.A. et al. (2008), *Equivalence of the waveguide invariant and two path ray theory methods for range prediction based on Lloyd's mirror patterns*, *Proceedings of Meetings on Acoustics*, **4**, 1, 6269–6273.
- KOZACZKA E., GRELOWSKA G. (2004), *Shipping noise*, *Archives of Acoustics*, **29**, 2, 169–176.
- LI J.B. (2012), *Regional Oceanography of China Seas Marine Geology*, China Ocean Press, Beijing.
- Ocean noise and marine mammals* (2003), Edited by Ocean Studies Board, National Academies Press (US), Washington (DC).
- ROSS D. (1987), *Mechanics of underwater noise*, Elsevier.
- SHEPARD F.P., EMERY K.O., GOULD H.R. (1949), *Distribution of sediments on East Asiatic continental shelf*, University of Southern California Press.
- URICK R.J. (1983), *Principles of underwater sound*, McGraw-Hill, New York.
- WALES S.C., HEITMEYER R.M. (2002), *An ensemble source spectra model for merchant ship-radiated noise*, *The Journal of the Acoustical Society of America*, **111**, 3, 1211–1231.
- WENZ G.M. (1962), *Acoustic ambient noise in the ocean: spectra and sources*, *The Journal of the Acoustical Society of America*, **34**, 12, 1936–1956.
- WESTON D.E. (1971), *Intensity-range relations in oceanographic acoustics*, *Journal of Sound and Vibration*, **18**, 2, 271–287, [https://doi.org/10.1016/0022-460X\(71\)90350-6](https://doi.org/10.1016/0022-460X(71)90350-6).
- WITTEKIND D.K. (2014), *A simple model for the underwater noise source level of ships*, *Journal of Ship Production and Design*, **30**, 1, 1–8.